

1
2
3
4
5
6
7
8
9
10
11
12
13
14
15
16
17
18
19
20
21
22
23
24
25
26
27
28
29
30
31
32
33
34
35
36
37
38
39
40
41
42
43
44
45
46
47
48
49
50
51
52
53
54
55
56
57
58
59
60
61
62
63
64
65

Seafloor Analysis and Understanding for Underwater Archaeology

Marco Reggiannini¹, Ovidio Salvetti¹

Via G. Moruzzi 1, Pisa

ISTI, CNR¹

Abstract

Surveying the oceans' floors represents at the same time a demanding and relevant task to operators concerned with marine biology, engineering or sunken cultural heritage preservation. Scientific researchers and concerned persons combine their effort to pursue optimized solutions aiming at the mapping of underwater areas, the detection of interesting objects and, in case of archaeological survey mission, the safeguard of the detected sites. Among the typical tools exploited to perform the cited operations the Autonomous Underwater Vehicles (AUVs) represent a validated and reliable technology. These vehicles are typically equipped with properly selected sensors that collect data from the surveyed environment. This data can be employed to detect and recognize targets of interest, such as manmade artefacts located on the seabed, both in an online or offline modality. The adopted approach consists in laying emphasis on the amount of regularity contained in the data, referring to the content of geometrical shapes or textural surface patterns. These features can be used to label the environment in terms of more or less interesting areas, where more interesting refers to higher chances of detecting the sought objects (such as man-made objects) in the surveyed area. This paper describes the methods developed to fulfill the purposes of mapping and object detection in the underwater scenario and presents some of the experimental results obtained by the implementation

URL: www.si.isti.cnr.it (ISTI, CNR)

¹Institute of Science and Information Technologies - National Research Council of Italy.

1
2
3
4
5
6
7
8
9 of the discussed techniques in the underwater archaeology field.

10 *Keywords:* Underwater Object detection, Optical and acoustic data
11 processing, Mosaicking, 3D reconstruction, Shape recognition, Texture analysis
12
13

14 1. Introduction

15
16
17
18 Mapping the oceans' floors represents an extremely demanding task to the
19 man. The peculiar environmental setting is for the most part out of reach to
20 human operators because of the hard environmental conditions that make the
21 survey complex and dangerous. Nevertheless the sea waters cover approximately
22 the 72% of the planet's surface and mapping the seafloors is still a relevant task
23 of typical concern to many involved operators such as biologists, engineers and
24 archaeologists.
25
26
27
28

29 On the other hand it is known that the oceans' floors host large amounts of
30 cultural heritage (more than 3 millions of wrecks according to the latest UN-
31 ESCO reports) as a consequence of shipwreckages that took place during the
32 past ages. This fostered the combined commitment between cultural institu-
33 tions and scientific researchers to pursue a solution towards the safeguard of
34 this collective patrimony. In this framework several ventures have been started,
35 based on the effort of either national (THESAURUS - TecnicHe per lEsplo-
36 razione Sottomarina Archeologica mediante lUtilizzo di Robot aUtonomi in Sci-
37 ami, PAR FAS 2007-2013 Regione Toscana) as well as international (ARROWS
38 - ARchaeological ROBot Systems for the World's Seas, European FP7 project)
39 cooperating consortia ([1], [2] and [3]). These projects have been focused on
40 the main purposes of mapping, diagnosing, cleaning and securing of underwater
41 and coastal archaeological sites. To perform all the cited operations a marine
42 vehicle, such as an autonomous underwater vehicle (AUV), can be profitably
43 exploited. The vehicle can be equipped with properly selected sensors, in order
44 to collect data from the surveyed environment in an optimal way.
45
46
47
48
49
50
51
52
53

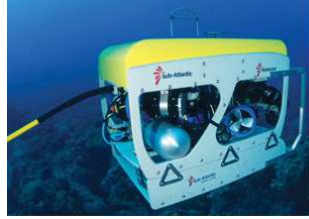
54 Typical sensors that turn out to be useful in this frame are optical cameras
55 coupled with acoustic sensors, like sidescan sonars or multibeam sonars. The
56
57
58
59
60
61
62
63
64
65

1
2
3
4
5
6
7
8
9
10
11
12
13
14
15
16
17
18
19
20
21
22
23
24
25
26
27
28
29
30
31
32
33
34
35
36
37
38
39
40
41
42
43
44
45
46
47
48
49
50
51
52
53
54
55
56
57
58
59
60
61
62
63
64
65

27 data collected by the AUVs during the mission campaigns can be processed in
28 order to detect targets of interest located on the seabed. The main approach
29 adopted in the processing procedure is to emphasize the amount of regular-
30 ity detected in the captured data, hence highlighting fragments of geometrical
31 shapes, such as primitive curves, or homogeneous areas exhibiting similar textu-
32 ral patterns. A strong and persistent presence of this regularities is considered
33 a clue for the presence of man made targets on the seafloor.

34 The features are computed by processing the optical and acoustic collected
35 data. The output result of the overall signal processing chain consists in the
36 labeling of the represented environment in terms of more or less interesting
37 scenarios. The term interesting usually refers to a quantitative index which
38 numerically expresses our confidence about the presence of some specific sought
39 object inside the environment. Hence it could be a score which, based on the
40 number and relevance of the detected features, could indicate the likely presence
41 of an interesting object. Given the generality of the proposed approach the
42 object to be detected can be represented by a large variety of targets, here
43 including archaeological wrecks as well as flora specimens, posidonia prairies or
44 corals or even underwater industry structures like oil and gas pipelines.

45 The methods developed to fulfill the cited purposes will be described in
46 detail in the remaining part of the paper, which is organized as follows: section
47 2 concerns a brief summary of the existing commercial solutions for underwater
48 vehicles, in section 3 the exploited sensors and their main features are discussed,
49 section 4 represents the paper's core and concerns the description of the main
50 approach and the multiple techniques developed to the purpose of understanding
51 and representing the underwater scenarios, finally section 5 concludes the paper
52 by discussing potential future prospects in the field of the underwater optical
53 and acoustic signal analysis.



a)



b)



c)



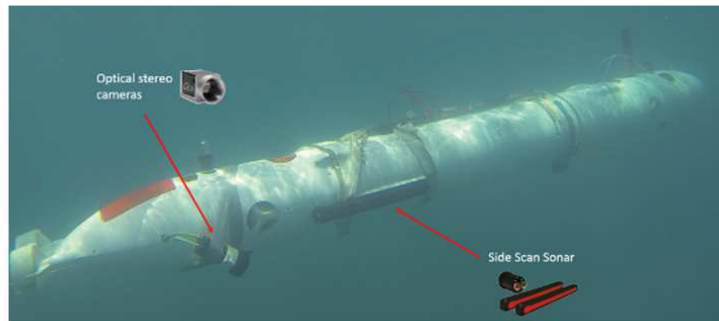
d)



e)



f)



g)

Figure 1: Sub-Atlantic Mohawk (a), an example of commercial ROV vehicle (picture available at <http://flowergarden.noaa.gov/>). Remus 100 (b), an example of commercial AUV (picture available at <http://hydroid.com/remus-100-marine>). Popular Commercial AUVs (c-f) and TifOne (g), the research AUV designed and implemented within the THESAURUS project. Details of the optical and acoustic payload mounting on TifOne are displayed.

2. Vehicle Platforms for Underwater Surveying

Among the technological systems employed to survey the underwater setting it is appropriate to spend a few considerations about the mobile platforms that are typically employed for maritime survey purposes and provide a brief presentation of their main properties and features. These mobile platforms can be roughly grouped in two classes: the Remotely Operated Vehicles (ROV, figure 1-a), that can be directly maneuvered by human operators thanks to a wired connection from a control platform to the vehicle itself, and vehicles that are designed to perform underwater missions without human supervision, i.e. the already mentioned AUVs (figure 1-b). In the following the latter category will be considered for further analysis since AUV has been chosen as the reference mobile platform for the marine survey tasks in THESAURUS and ARROWS. Among the most relevant outcomes of the mentioned projects several solutions of AUVs specifically dedicated to the archaeological exploration task have been designed, implemented and experimentally tested.

AUVs are programmable robotic vehicles that, depending on their design, can drive or glide through the ocean without the requirement of a real-time control by human operators. When needed AUV's control and localization may be performed by means of acoustic communication channels towards surface platforms or by exploiting underwater positioning methods based on networks of acoustic beacons distributed on the seafloor, such as Long, Short or Ultrashort Baseline technologies ([4]). Otherwise, once the mission has started the vehicle performs the planned tasks autonomously, without interacting with human operators until the end of the mission.

Most of the available AUVs feature a torpedo-like shape. They are often employed as multi-purpose platforms for oceanographic experiments since they can be quite easily deployed in the marine environment and activated to perform specific measurements. The main components that make up an AUV are:

- i) an essential system resulting from the combination of the chassis structure and all the engineering systems governing the mechanical behaviour (propellers,

1
2
3
4
5
6
7
8
9
10
11
12
13
14
15
16
17
18
19
20
21
22
23
24
25
26
27
28
29
30
31
32
33
34
35
36
37
38
39
40
41
42
43
44
45
46
47
48
49
50
51
52
53
54
55
56
57
58
59
60
61
62
63
64
65

84 actuators, etc.), here including a primary processing unit assigned to the im-
85 plementation and control of basic tasks (navigation and attitude control, inter-
86 nal humidity measurement and generic vehicle diagnostics), ii) a data capture
87 system resulting from the integration of hardware tools (payload sensors) and
88 software modules (ad hoc implemented data processing algorithms) dedicated
89 to the tasks of surveying and understanding the environment. Installation of
90 payload sensors can be adapted according to different mission scenarios, from
91 physical parameters measurement such as CTD probing (conductivity, temper-
92 ature and depth/pressure profiling), to inspections of the environment by means
93 of optical and acoustic mapping sensors (TV cameras and side scan sonar).

94 Existing AUVs feature strong pressure resistance, an important property
95 that allows to reach relevant depths, typically from hundreds to thousands of
96 meters. This enables the system to perform large scale mapping of vast areas
97 as well as close-up inspections of the seafloor.

98 So far a large number of commercial solutions have been proposed by com-
99 panies operating in the maritime field. REMUS (figure 1-b,c) represents one of
100 the most popular typologies of AUV. It is produced by Hydroid, which is part
101 of Kongsberg Maritime Company (Norway). Its length varies from 1.6 m (RE-
102 MUS 100) to 3.84 m (REMUS 6000) and it is rated for a maximum operating
103 depth of 100 m (REMUS 100) to 6000 m (REMUS 6000). Its battery ensures a
104 mission duration of 10 hours (REMUS 100) to 22 hours (REMUS 6000) and a
105 maximum speed of 2.3 m/s.

106 Hydroid is also the manufacturer of HUGIN (figure 1-d), another commercial
107 AUV which is suitable for underwater inspection and mapping purposes. Its
108 specifications are very similar to the REMUS ones, differing only for its larger
109 dimensions (up to 6.4 m) and better performances in terms of battery endurance
110 (up to 74 hours).

111 The mentioned vehicles represent interesting solutions given their versatility
112 for applications to a wide range of underwater operations, from pipeline moni-
113 toring to mine countermeasure missions, here including mapping for biological
114 inspection and geological assessment purposes. The main drawbacks of the de-

1
2
3
4
5
6
7
8
9
10
11
12
13
14
15
16
17
18
19
20
21
22
23
24
25
26
27
28
29
30
31
32
33
34
35
36
37
38
39
40
41
42
43
44
45
46
47
48
49
50
51
52
53
54
55
56
57
58
59
60
61
62
63
64
65

115 scribed systems are represented by their relevant cost (from 100K€ to 1M€)
116 and by their voluminous dimensions (HUGIN may weigh up to 1550 Kg), which
117 make them impracticable for operations carried out by small groups of people
118 and implies the rental of expensive dedicated machinery and supporting ships
119 in order to perform a safe and proper deployment.

120 Many companies provide solutions that can be considered relatively comfort-
121 able in terms of transport and deploy, such as the OceanServer IVER-3 (figure
122 1-e) or the modular Teledyne GAVIA (figure 1-f). Both the vehicles have an
123 approximating length of 2 meters and a weight of about 50 Kg. The additional
124 modularity feature of the Teledyne GAVIA enables the user to adapt the vehi-
125 cle to the experimental requirements, by installing onboard the proper payload
126 sensor modules. This represents a crucial requirement, that inspired the me-
127 chanical design activity within both projects, THESAURUS and ARROWS.
128 Indeed modularity represents a desirable condition in order to make the sen-
129 sor platform versatile and adaptive to different mission scenarios, such as the
130 strongly varying altitude parameter (distance of the vehicle from the seafloor)
131 that typically differentiates between large scale survey missions (e.g. 40 m alti-
132 tude) or close range observations of localized spots (few meters altitudes).

133 The following sections concern a detailed description of the engineering and
134 information technology results achieved within the research projects previously
135 introduced, representing the scientists' answer to the lack of current market
136 solutions dedicated to the fulfillment of archaeologists' desiderata. This is true
137 for what concerns the lack of embedded software systems for the processing,
138 integration and understanding of the captured payload sensor data, aiming at
139 the discovery of currently undetected underwater archaeological sites.

140 **3. AUV Sensor Equipment for Optimal Data Acquisition**

141 In the circumstances described in this paper the AUV is equipped with
142 sonars and optical cameras in order to map the seafloors. More in detail the
143 sensing system features two digital cameras in stereo configuration with a sonar

1
2
3
4
5
6
7
8
9
10
11
12
13
14
15
16
17
18
19
20
21
22
23
24
25
26
27
28
29
30
31
32
33
34
35
36
37
38
39
40
41
42
43
44
45
46
47
48
49
50
51
52
53
54
55
56
57
58
59
60
61
62
63
64
65

144 device, which can be a multibeam or a side scan sonar. The choice of the
145 acoustic payload sensors to be employed during the missions depends on the
146 specific purpose of the mission itself and on the environmental scenario that has
147 to be surveyed. The side scan sonar and the multibeam forward looking sonar
148 return large scale maps of the seafloor that are typically processed to detect
149 obstacles, objects or areas of the seafloor showing interesting features. On the
150 other hand the multibeam echosounder returns detailed 3D bathymetry maps
151 of the inspected area in the form of point cloud data.

152 Typically optical and acoustic sensors are installed on the same AUV, they
153 share the vehicle reference frame and capture co-located data, that is they re-
154 turn a multi-sensor description of the environment from a common perspective.
155 Considering the object detection as a primary goal for this work, the selected
156 sensor suite turns out to be the optimal choice. Indeed optical and acoustic de-
157 vices feature complementary properties in terms of resolution and best operating
158 conditions.

159 An example of a research-oriented AUV, equipped with optical and acoustic
160 payload sensors, is represented in figure 1-f, displaying the TifOne, an AUV that
161 has been developed by the Mechatronics and Dynamic Modelling Laboratory of
162 the University of Florence in the framework of the ARROWS project.

163 Due to the complex and noisy environment in which the survey operations
164 are performed, the data collected by the payload sensors must undergo multi-
165 ple processing stages, starting from the enhancement of the raw output signal,
166 ending with specific computer vision and image processing techniques with the
167 purpose of extracting as much information as possible from the collected data.
168 A preliminary step in the manipulation of the data consists in the restoration of
169 the signal and in the enhancement of the relevant properties, whose integrity is
170 crucial for the correct understanding of the scenario. In our specific case we are
171 concerned with correcting those systematic geometrical distortions introduced
172 in the signal due to the peculiar perception of the environment, which is intrinsic
173 in every employed sensor.

174 As an example consider the geometrical distortions affecting the side scan

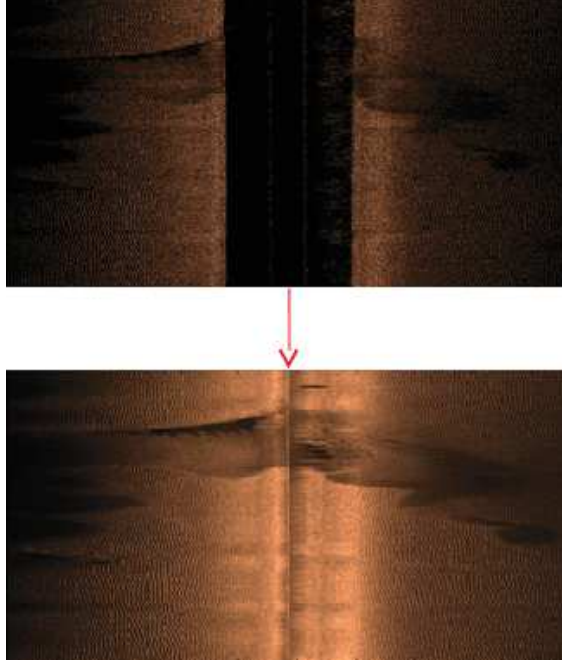


Figure 2: Side scan sonar map represented by Slant (up) and Ground (down) corrected coordinates.

sonar mapping: the measured time of the backscatter echo is not linearly proportional to the seabed ground range. Indeed, within a row of a Side Scan Sonar map, different segments of pixels with the same given length, starting from different positions of the row, correspond to spatial segments with different lengths on the horizontal (ground) range axis. To correctly represent the data in the seabed frame the *Slant-to-Ground* transformation indicated below is required:

$$y_{i,j} = \sqrt{\frac{c^2 t_{i,j}^2}{4} - H_i^2} \quad (1)$$

where $y_{i,j}$ is the j -th horizontal range sample in the i -th ping, c is the sound velocity in the sea, $t_{i,j}$ is the j -th slant range (time) sample in the i -th ping and H_i is the first echo return of the i -th ping, i.e. the sensor i -th altitude value. Besides the transform in equation (1) allows to get rid of the

1
2
3
4
5
6
7
8
9
10
11
12
13
14
15
16
17
18
19
20
21
22
23
24
25
26
27
28
29
30
31
32
33
34
35
36
37
38
39
40
41
42
43
44
45
46
47
48
49
50
51
52
53
54
55
56
57
58
59
60
61
62
63
64
65

185 central black stripe in the raw output sonogram, which is caused by the acoustic
186 wave propagation through the water column (figure 2).

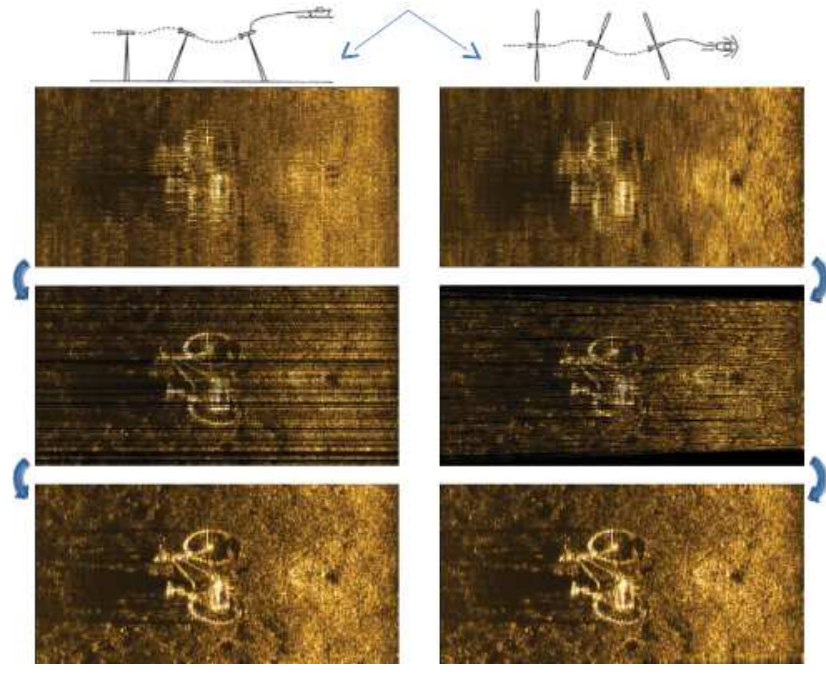


Figure 3: Sidescan sonar map: altitude distortions and corresponding restoration. Original side scan map available on <http://www.jfishers.com/>.

187 Relevant sources of image distortion come from the random distortions in
188 the sonogram formation, caused by the unpredictable fluctuations in the AUV
189 attitude (figure 3).

190 In both the mentioned examples auxiliary sensor devices, such as inertial
191 measurement units, gyrocompass, DVL, etc., can be exploited to provide the
192 vehicle's position and pose values during the payload acquisition. This addi-
193 tional information can be profitably used to restore the corrupted data (see for
194 example [5]). Results of the restoration are presented in the lower part of figure
195 3.

196 In the underwater mapping field the signal pre-processing stage represents

1
2
3
4
5
6
7
8
9
10
11
12
13
14
15
16
17
18
19
20
21
22
23
24
25
26
27
28
29
30
31
32
33
34
35
36
37
38
39
40
41
42
43
44
45
46
47
48
49
50
51
52
53
54
55
56
57
58
59
60
61
62
63
64
65

197 an important step to be performed before applying algorithms aiming at a high
198 level understanding of the surveyed scenario. Indeed the performance of an
199 automatic understanding system, which involves algorithms borrowed from the
200 computer vision, machine learning and image processing background, strongly
201 depends on the quality of the captured data. Actually we have to be confident
202 that the data, either considered as a straight raw output of the sensor or as
203 the result of the preprocessing stages, exhibit the highest achievable quality.
204 This is an auspicious precondition, that should be pursued in order to allow the
205 dedicated processing units to automatically detect those features and attributes
206 of conspicuous importance for the understanding process.

207 **4. Analysis of the Captured Data and Underwater Scene Understand-**
208 **ing**

209 A mixture of unfavourable factors makes the collection of reliable data in the
210 underwater setting a hard task: due to the perturbations' spherical spreading
211 the optical and acoustic energy collected by the sensors decreases proportionally
212 to the squared inverse of the travelled distance.

213 Moreover the underwater medium heavily affects the spectrum of the optical
214 signal by filtering out a large percentage of the visible frequency range ([6] and
215 [7]). This reduces the maximum operational range of the optical sensor to few
216 meters. Underwater imaging is also corrupted by typical hazing effects that may
217 strongly reduce the visibility in the image.

218 *4.1. Mosaicking*

219 The described sensing limitations can be tackled in case a large set of data
220 relating to the same scenario is available. By exploiting computer vision algo-
221 rithms that perform the alignment and the integration of multiple maps it is
222 possible to generate a representation of the entire surveyed environment. This
223 can be obtained by exploiting mosaicking procedures. These techniques start
224 from the hypothesis that the surveyed environment features a planar morphol-
225 ogy or can be approximated as planar from the camera point of view. Let's

1
2
3
4
5
6
7
8
9
226 consider a point x in multiple consecutive maps resulting from the projections
10
227 onto the camera plane of the same 3D world point. Under the hypothesis that
11
228 the different images are related by a projective transformation (homography in
12
229 case of planar projection), the relation between the point coordinates in image
13
230 i and j can be formally expressed as:

$$\mathbf{x}_i \sim \mathbf{H}_{i,j} \mathbf{x}_j \quad (2)$$

20
21
22 where $H_{i,j}$ represents the homography transform that maps points of image
23
232 j on image i . In case of projections of 3D points on the camera plane the
24
233 homography is usually represented by a 3×3 matrix with 8 degrees of freedom.

25
26
234 The homography can be estimated directly from the captured images by
27
235 considering 3 conditions for every interest point, defined by equation (2). Given
28
236 n points we have $3n$ equations and $8 + n$ unknown (scale unknown has to be
29
237 considered if we perform the estimation exploiting points from the captured
30
238 cameras), so we must have at least 4 points to correctly estimate $H_{i,j}$.

31
32
33
239 The x points are usually selected based on the detection of reliable fea-
34
240 tures in the data, such as SIFT features ([8]). The features that are detected,
35
241 matched and exploited to estimate $H_{i,j}$ correspond to those features appearing
36
242 in the overlapping areas of consecutive maps. The transformed maps are finally
37
243 stitched together and eventually processed by blending techniques to generate
38
244 a final seamless mosaic map.

39
40
41
42
43
245 In the unfavourable case that the number of detected reliable features is too
44
246 low due to bad quality or very noisy data the feature based mosaicking may
45
247 become an unfeasible operation.

46
47
48
248 Under that condition the additional data collected by auxiliary sensors mea-
49
249 suring the vehicle attitude may help towards the estimation of the required
50
250 transformations.

51
52
251 In the framework of the ARROWS project the mosaicking procedure based
53
252 on a feature matching approach has been tested on a set of acoustic and optical
54
253 data captured during experimental campaigns performed in Sicily and Israel.

1
2
3
4
5
6
7
8
9
10
11
12
13
14
15
16
17
18
19
20
21
22
23
24
25
26
27
28
29
30
31
32
33
34
35
36
37
38
39
40
41
42
43
44
45
46
47
48
49
50
51
52
53
54
55
56
57
58
59
60
61
62
63
64
65



Figure 4: Optical mosaic map. The image results from the stitching process of 61 frames captured by a Basler ACE GigE camera during an experimental campaign performed at the Cala Minnola site, in front of the Levanzo Island, Sicily.

254 During a mission at the Levanzo Island, in Sicily a set of optical images has
255 been captured at the Cala Minnola site and have been processed to return an

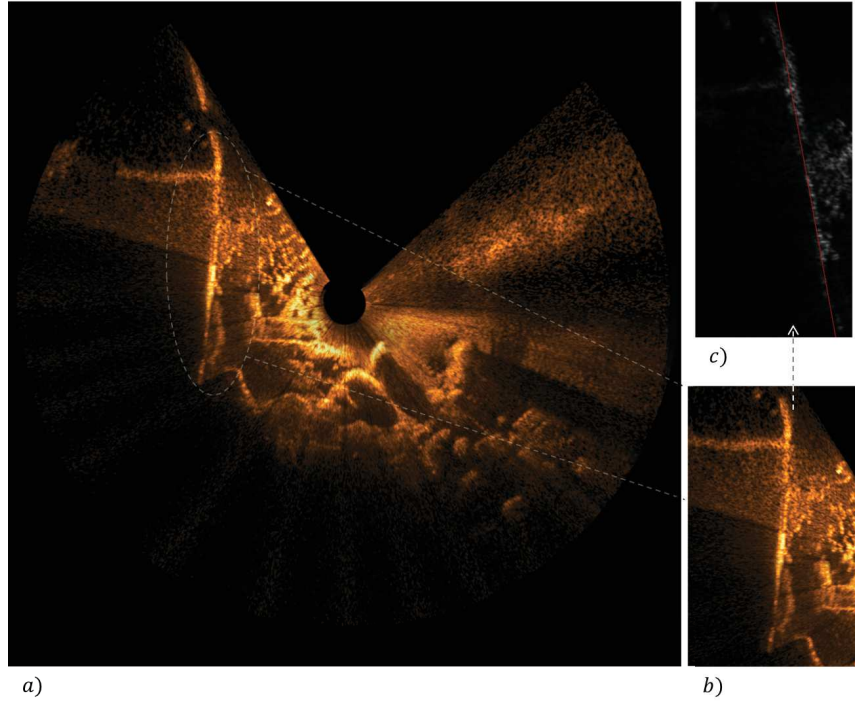


Figure 5: Image a): Forward Looking Sonar mosaic map. The image results from the stitching process of 17 frames captured by a Blueview MB P900 sonar during an experimental campaign performed in Israel, at the Caesarea ancient harbour. Image b): Linear detail, belonging to a pier wall structure, of the mosaic map on the left. Image c): The linear structure represented in image b) has been detected by means of the geometry detection techniques described in this paper.

256 overall map of the archaeological scene, as illustrated in figure 4. The same pro-
 257 cedure has been tested during the Israel campaign. In the latter circumstance
 258 a multibeam forward looking sonar sensor (Blueview MB-P900) has been em-
 259 ployed to survey a pier wall in the nearness of the Caesarea harbor. Part of the
 260 captured data has been processed to obtain a large scale map of that area, as
 261 illustrated in figure 5-a.

1
2
3
4
5
6
7
8
9
262 *4.2. Geometry presence assessment*

10
11
12
13
14
15
16
17
18
19
20
21
22
23
24
25
26
27
28
29
30
31
32
33
34
35
36
37
38
263 A relevant activity has been developed bearing in mind the primary goal
264 of an archaeological mission, that is the detection of potential structures re-
265 lated to human made objects. The automated system that should perform this
266 task, must recognize specific features exhibited by the selected candidates and
267 put forward an hypothesis on the manmade object's nature. Hence a set of
268 proper criteria has to be chosen in order to grab the most relevant objects'
269 attributes. Within the multiple possible choices we oriented our approach to-
270 wards assessing the presence of regularity features contained in the captured
271 data. These regularity attributes may refer to the geometric shapes that define
272 the contours of objects as perceived by the sensor device, hence fragments of
273 primitive curves such as lines, circles or ellipses. Starting from the hypothesis
274 that a high concentration of regular curves is a marker for the presence of man-
275 made objects or shipwrecks, we focused our work on the automatic detection
276 of elementary geometric features (line segments, elliptical arcs) in images. This
277 represents a classical computer vision issue which has been thoroughly tackled
278 and discussed by the scientific community (see for example [9] and [10]). The
279 current procedures for geometric features recognition can be roughly classified
280 into Hough-based and region chaining methods.

39
40
41
42
43
44
45
46
47
48
49
50
51
52
53
54
55
56
57
58
59
60
61
62
63
64
65
281 The Hough-based algorithms make use of implementative variations of the
282 Hough transform. These methods ensure that pixels belonging to the same geo-
283 metric structure are mapped to the same point into a parameter space whose
284 dimensionality is given by the number of parameters. This typology of al-
285 gorithms implies elevated computational costs since the procedure complexity
286 grows proportionally with the number of the curve parameters. Therefore it
287 is a good choice to detect lines, but not to detect circular or elliptical shapes.
288 In the authors experience Hough based procedures have been useful to detect
289 the presence of structures featuring mostly linear shapes, such as architectural
290 elements or remains of ancient walls. An example comes from the Israel mission
291 mentioned in section 4.1: the captured acoustic dataset has been processed to
292 detect the presence of primitive curves and the result is illustrated in figure 5-c,

1
2
3
4
5
6
7
8
9
10
11
12
13
14
15
16
17
18
19
20
21
22
23
24
25
26
27
28
29
30
31
32
33
34
35
36
37
38
39
40
41
42
43
44
45
46
47
48
49
50
51
52
53
54
55
56
57
58
59
60
61
62
63
64
65

293 where the red line identifies a pier wall structure (detailed in figure 5-b) detected
294 by the algorithm.

295 The second class of detection methods relies on region growing and chaining
296 techniques. This method exploit the geometric properties of the shapes directly
297 assessed from the images, such as straightness for line segments or curvature
298 properties for ellipses.

299 These algorithms usually start with a seed pixel or a group of pixels. Then
300 additional pixels are added, provided that they obey some geometric properties
301 of the candidate shape. For example a pixel with coordinates \mathbf{p} and intensity
302 $x(\mathbf{p})$ can be considered aligned to an elliptical arc a if the angle θ formed by
303 the normal $\mathbf{n}_a(\mathbf{p})$ to the arc and the image gradient falls below a predetermined
304 threshold θ_{th} , as expressed by equation (3) and illustrated in figure 6:

$$\theta(\nabla x(\mathbf{p}), \mathbf{n}_a(\mathbf{p})) \leq \theta_{th} \quad (3)$$

305 Starting from the work presented in [11] we implemented a procedure for
306 primitive curves recognition purposes. The Ellipse and Line Segment Detector
307 (ELSD) algorithm described in that paper is based on the Gestalt theory, whose
308 applications to computer vision issues are thoroughly discussed in [12]. In a
309 nutshell this method is based on the so called *Helmoltz's perception principle*

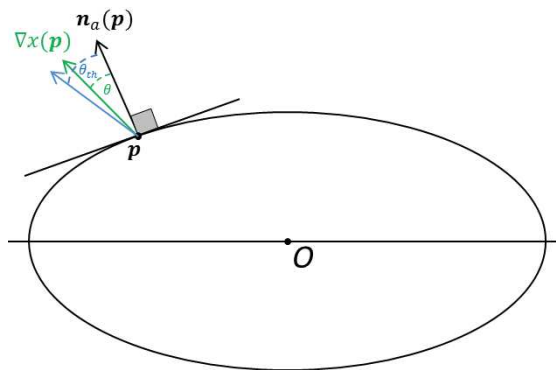


Figure 6: Elliptical collinearity condition.

1
2
3
4
5
6
7
8
9
10
11
12
13
14
15
16
17
18
19
20
21
22
23
24
25
26
27
28
29
30
31
32
33
34
35
36
37
38
39
40
41
42
43
44
45
46
47
48
49
50
51
52
53
54
55
56
57
58
59
60
61
62
63
64
65

310 which formally states that in an unstructured image, only a very small number
311 of detections (false alarms) should take place. The decision about a meaningful
312 candidate curve is based on the probability of observing candidates as structured
313 as the considered one: the smaller this probability value is, the more meaningful
314 the candidate curve is to be considered.

315 More details about the implemented curve recognition procedure and its
316 application to archaeological sites detection can be found in [13], [14]. This
317 technique can also be exploited on sonar maps to perform attentive analysis of
318 the data (figure 7). By applying the curve recognition algorithm to the new
319 maps, as soon as they become available during the mission, an instantaneous
320 label of interest is assigned to the surveyed regions. Based on that the system
321 can autonomously decide in real time whether a specific area is worth of more
322 detailed inspection or not.

323 Once more it is worth reminding that a correct restoration of the signal, as
324 illustrated in figure 3, may affect critically the curve recognition process. This
325 is even more important in case the surveyed environment features large varieties
326 of shapes and contours, such as archaeological sites including amphoras, plates
327 and complex wrecks.

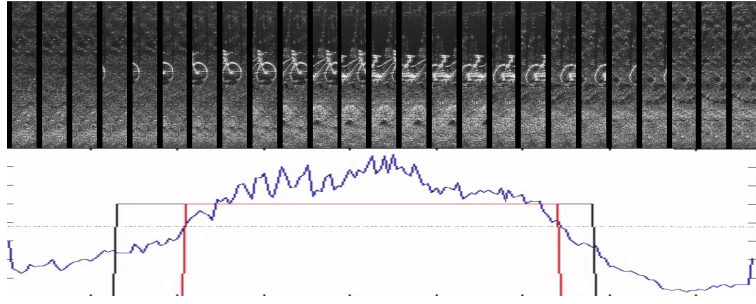


Figure 7: Attentive analysis procedure based on geometry detection applied to the side scan sonar map of figure 3. The blue curve growth is proportional to the number of detected curves, the red line represents the threshold over which the detected number of curves is to be considered relevant and the black line represents a ground truth reference.

1
2
3
4
5
6
7
8
9
328 *4.3. Texture analysis*

329 As previously mentioned, this work is mainly concerned about detecting
330 regularity features in the captured data. Besides shape information, the regu-
331 larity in terms of *textural* features can be exploited to group pixels of an image
332 in classes that share similar patterns. In this sense the surface appearance of
333 the objects located in the surveyed environment is the attribute that can be
334 exploited to perform image segmentation and classification.

335 More in particular the appearance of an object's surface can be represented
336 in the spatial frequency domain and the surface patterns may be classified by
337 exploiting their specific frequency content, which plays therefore the role of a dis-
338 criminative signature. A mathematical tool that has been successfully employed
339 to perform this operation is the 2D Gabor wavelet function, whose mathematical
340 definition is expressed by equation 4.

$$h(x, y) = \exp \left[-\frac{1}{2} \left(\frac{x^2}{\sigma_x^2} + \frac{y^2}{\sigma_y^2} \right) \right] \cos(2\pi u_0 x) \quad (4)$$

341 The wavelet orientation can be adjusted by properly rotating the coordinate
342 system, as in equation 6.

$$x' = x \cos \theta_0 + y \sin \theta_0 \quad (5)$$

$$y' = -x \sin \theta_0 + y \cos \theta_0 \quad (6)$$

343 In the Fourier domain the transformed Gabor wavelet is represented as a 2D
344 Gaussian function centered at the specific u_0 radial frequency value. From a
345 signal processing point of view the Gabor wavelet can be considered a bandpass
346 filter centered on the specific wavelet band.

347 The convolution with the Gabor wavelet, which is performed on small win-
348 dows centered on the image pixels, becomes a multiplication between the trans-
349 formed functions in the Fourier domain and this results in the emphasis of the
350 common frequency components. This operation is repeated by varying u_0 and
351 θ_0 , then, for every convolution result, specific features are computed, such as

1
2
3
4
5
6
7
8
9
10
11
12
13
14
15
16
17
18
19
20
21
22
23
24
25
26
27
28
29
30
31
32
33
34
35
36
37
38
39
40
41
42
43
44
45
46
47
48
49
50
51
52
53
54
55
56
57
58
59
60
61
62
63
64
65

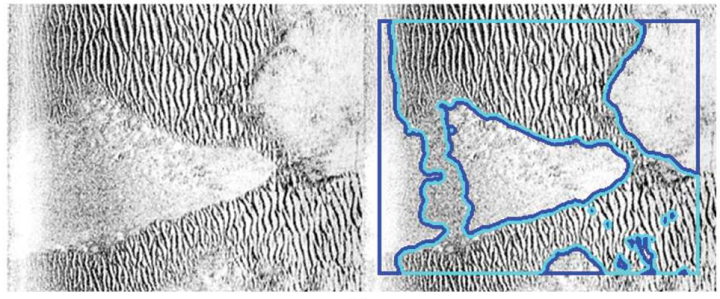
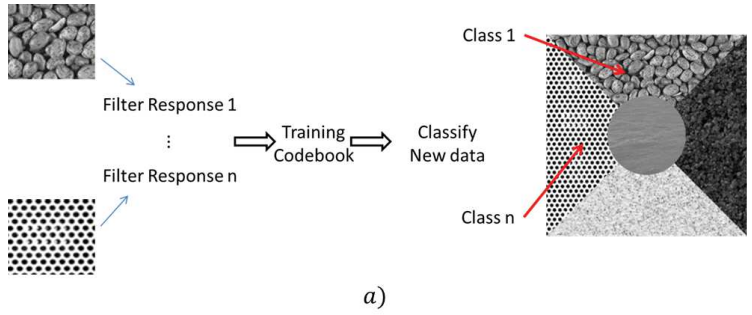


Figure 8: Image a): Preliminary training for the texture classification algorithm (original image taken from <http://note.sonots.com/>). Image b): Texture classification of side scan sonar maps by means of Gabor filtering (original image taken from <http://www.ise.bc.ca/>).

352 the energy of the filtered image, as in [15]. Hence for every image pixel we
353 obtain a set of features describing the pixel frequency content. The similarity
354 between pixels is assessed by comparing the computed feature vectors by means
355 of a proper proximity criterion. To this aim popular clustering algorithms, like
356 K-means (see for example [16]), can be successfully employed. The final seg-
357 mentation of the map is performed by repeating the described operation for
358 every pixel.

359 The algorithm can be executed as an unsupervised procedure where the clus-
360 ter centroids are estimated iteratively from the data, by applying techniques as
361 the cited K-means. An advanced implementation is based on a preliminary
362 training stage in which a set of known classified patterns are processed with dif-

1
2
3
4
5
6
7
8
9
363 ferent Gabor wavelets in order to provide the main spectral features for various
10
11 364 classes, such as rock, sand, mud, posidonia, etc. The results obtained this way
12
13 365 are then used to train the algorithm, which is later employed to classify areas
14
15 366 in new captured data, based on the increased a priori knowledge. A conceptual
16
17 367 sketch of this procedure is represented in figure 8-a and a result of the seg-
18
19 368 mentation process applied on real side scan sonar data is represented in figure
20
21 369 8-b.

20
21 370 This way it is expected that the resulting process may be employed also for
22
23 371 online purposes, aiming at a fast preliminary classification of the environment
24
25 372 to quickly identify the interesting spots.

26 373 4.4. 3D Reconstruction

27
28 374 The techniques described so far allow to perform a large scale mapping of
29
30 375 the seafloor. This is an important step since in the first instances of the survey
31
32 376 operations the main goal is that of detecting those regions of the seabed that
33
34 377 feature high probabilities for the presence of archaeological objects. Once a
35
36 378 certain area has been identified a dedicated survey on the localized spot must be
37
38 379 performed. The data captured during this close-range survey can be employed
39
40 380 for an offline stage of signal processing, aiming at the generation of 3D models
41
42 381 of the interesting targets.

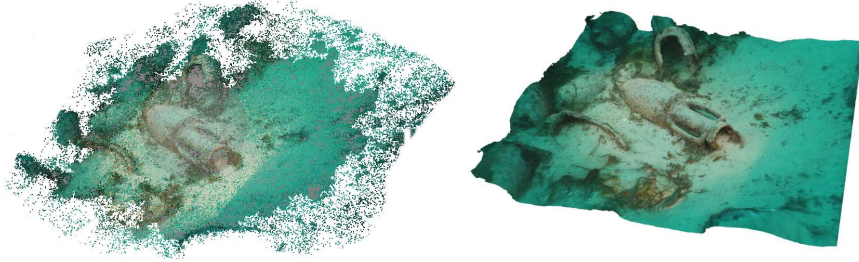
40
41 382 Accurate 3D models of the objects can be obtained by processing optical data
42
43 383 by advanced photogrammetry methods, such as Structure From Motion (see [17]
44
45 384 and [18]). This method is based on the estimation of the 3D coordinates of a
46
47 385 point \mathbf{X}_i from the projection \mathbf{x}_{ij} of the point itself on the multiple image planes,
48
49 386 defined by the subscript j . The link between \mathbf{X}_i and the point \mathbf{x}_{ij} , identifying
50
51 387 the projection on the j -th image, is expressed by:

$$52 \lambda_j \mathbf{x}_{ij} = \mathbf{P}_j \mathbf{X}_i \quad (7)$$

53
54 388 where the *camera matrix* \mathbf{P}_j represents our knowledge about the camera
55
56 389 intrinsic parameters (aspect ratio, skew, focal length and camera center co-
57
58 390 ordinates) and the camera extrinsic parameters (the rotation and translation

60
61
62
63
64
65

1
2
3
4
5
6
7
8
9
391 transforms that define the camera pose and position with respect to a global
392 world reference frame). λ_j is a scale factor which accounts for the representation
393 of the image point \mathbf{x}_{ij} in homogeneous coordinates.



24
25
26
27
28
29
30
31
32
33
34
35
36
37
38
39
40
41
42
43
44
45
46
47
48
49
50
51
52
53
54
55
56
57
58
59
60
61
62
63
64
65
Figure 9: 3D sparse point cloud (left) and refined mesh (right) of an amphora generated from optical data. The image displays a detail of the Cala Minnola wreck site, an underwater archaeological site that has been surveyed in the experimental mission performed in the ARROWS project framework.

394 It is presumed that the projections of \mathbf{x}_i on different images are recognized
395 as generated from the same spatial point. This can be performed by methods
396 for the detection and matching of salient features, as the SIFT method touched
397 in the 4.1 paragraph. The computation is performed by exploiting multiple
398 constraints on the \mathbf{x}_i , resulting from equation (7), expressed for different camera
399 poses j . The estimation of the point coordinates and camera matrices results in
400 the generation of a 3D point cloud, such as the one on the left side of figure 9.

401 The result can be further refined by estimating the dense cloud and, later,
402 the mesh surface fitting the point cloud. This can be performed by exploiting
403 popular open source softwares such as Meshlab ([19]). An example of point
404 cloud processing is illustrated on the right side of figure 9.

405 Another typical way of obtaining 3D bathymetric data in the underwater
406 environment is by employing acoustic multi-beam sonars. The output data
407 returned by the multibeam sonar consists of a set of 3D points lying in the
408 intersection between the acoustic beams and the seafloor plane. The depth
409 values and the direction of arrival of the scatterers are hence the direct output

1
2
3
4
5
6
7
8
9
10
11
12
13
14
15
16
17
18
19
20
21
22
23
24
25
26
27
28
29
30
31
32
33
34
35
36
37
38
39
40
41
42
43
44
45
46
47
48
49
50
51
52
53
54
55
56
57
58
59
60
61
62
63
64
65

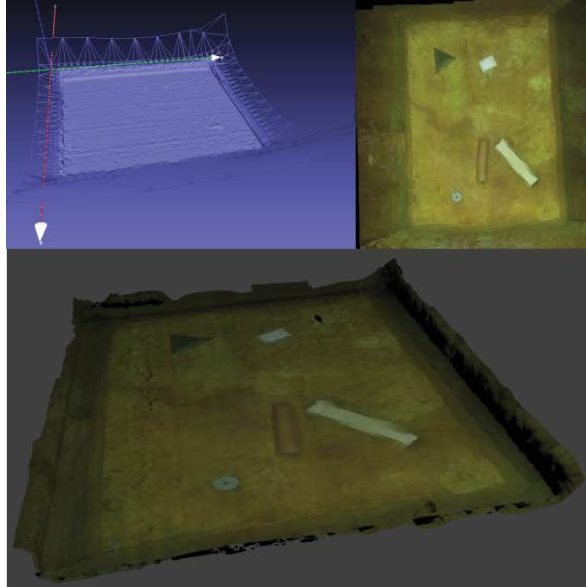


Figure 10: Heterogeneous dataset captured during an experimental session at the small pool of the Ocean Systems Lab, Heriot Watt University (Edinburgh). In the left upper part the pool bathymetry map captured by the Blueview MB2250 is illustrated. The right upper part represents the optical mosaic obtained by stitching the GoPro images of the pool floor while the lower part represents the integration between the bathymetric map and the optical mosaic.

of this sensor. This information can be integrated with additional sensor pose
and position measurements. This enables the generation of 3D point cloud of
the environment. The mapping performance of a Blueview MB-2250 multibeam
sonar has been tested by collecting an experimental dataset within the small
pool environment of the Ocean Systems Laboratory, Heriot Watt University of
Edinburgh (Scotland). The collected maps have been processed to extract the
linear subset of interest from the data, corresponding to the intersection between
the sensor beams and the pool floor. Later, by integrating these data with the
pose measurements of the sensor, it was possible to perform the 3D alignment of
the point cloud. The point cloud obtained this way has been further processed
to generate the 3D mesh of the terrain (figure 10, upper left), and the result has
been integrated with the optical mosaic of the floor (figure 10, upper right). The

1
2
3
4
5
6
7
8
9
10
11
12
13
14
15
16
17
18
19
20
21
22
23
24
25
26
27
28
29
30
31
32
33
34
35
36
37
38
39
40
41
42
43
44
45
46
47
48
49
50
51
52
53
54
55
56
57
58
59
60
61
62
63
64
65

422 optical dataset has been obtained by employing a GoPro camera, collecting data
423 simultaneously with the MB-2250. The result of the fusion between bathymetry
424 and textural information is represented in the lower part of figure 10.

425 4.5. Data Integration

426 During the survey missions each of the employed payload sensors will pro-
427 vide an individual description of the environment. To the purpose of robustly
428 recognizing archaeological objects it is useful to introduce a synthesis structure
429 summarizing all the informative content related to a seabed area.

430 This can be formally defined as a multi-dimensional map, made up of multi-
431 ple layers, each of which refers to a specific category of information. A point in
432 this map returns the entire available information for the corresponding 3D point
433 in the world ([20]). This information may refer to (i) the raw captured data,
434 (ii) the output results of data analysis algorithms, (iii) the bathymetry data
435 collected by dedicated sensors or estimated by computer vision procedures. A
436 point in the map \mathbf{p} can be formally defined as an n -D vector, where n represents
437 the dimensionality of the collected information, which varies with the number
438 of employed payload sensors and the implemented algorithms for data analysis:

$$\mathbf{p}(x, y) = \{p_1(x, y), \dots, p_n(x, y)\} \quad (8)$$

439 According to the previous definition, an example of the multi dimensional
440 map that would realistically represent the output of an AUV archaeological
441 mission, could be built as in the following:

$$\begin{aligned} p_1(x, y) &= \text{Optical Map Intensity value in } (x, y) \\ p_2(x, y) &= \text{Acoustic Map Intensity value in } (x, y) \\ &\dots \\ p_n(x, y) &= \text{Bathymetry Map value in } (x, y) \end{aligned} \quad (9)$$

442 A conceptual sketch of the described fusion map is illustrated in figure 11. In
443 comparison with object recognition procedures based on an individual data ty-

1
2
3
4
5
6
7
8
9
10
11
12
13
14
15
16
17
18
19
20
21
22
23
24
25
26
27
28
29
30
31
32
33
34
35
36
37
38
39
40
41
42
43
44
45
46
47
48
49
50
51
52
53
54
55
56
57
58
59
60
61
62
63
64
65

444 pology, it is expected that considering the whole set of available information can
445 be a promising way to perform an efficient object recognition task, reliable with
446 respect to false alarms rejection. A preliminary example of data integration, re-
447 sults from the stitching of camera images mosaic on the multibeam bathymetry
448 map (figure 10). Future work will involve enlarged sets of heterogeneous data
449 and it will be performed on the real data that will be captured during the final
450 experimental surveys of the ARROWS project.

451 5. Conclusions

452 The robotic and automation technology presented in this paper will make
453 easier the underwater archaeologists' work, carried out in a hostile and complex
454 environment.

455 The many implemented procedures aim at providing the archaeologists with
456 methods to perform a thorough analysis of the large and heterogenous amount
457 of data returned by the payload sensors. The proposed processing options aim
458 at the fulfillment of all the archaeologist's requirements and enable him to in-
459 directly perform measurements and formulate historical interpretations on the
460 findings. Moreover, in order to disseminate knowledge regarding the underwater
461 cultural heritage and to increase the sensitivity for its preservation, the devel-

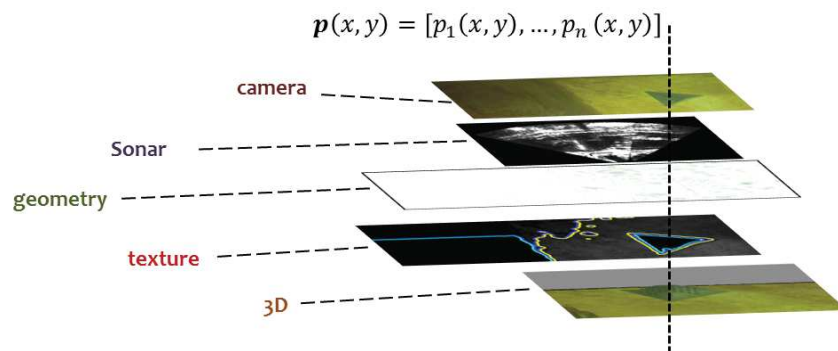


Figure 11: Conceptual diagram illustrating the fusion map. A point in the multilayer structure summarizes all the available information about the surveyed environment.

1
2
3
4
5
6
7
8
9
10
11
12
13
14
15
16
17
18
19
20
21
22
23
24
25
26
27
28
29
30
31
32
33
34
35
36
37
38
39
40
41
42
43
44
45
46
47
48
49
50
51
52
53
54
55
56
57
58
59
60
61
62
63
64
65

462 oped tools allow to address different audiences, including the general public. In
463 particular, one of the purposes of this work is to devise new dissemination chan-
464 nels making use of 3D immersive environments to make more attractive the col-
465 lected information. The developed methodology has been tested by organizing
466 specific campaigns in relevant European sites, such as the Egadi Archipelagos
467 in Italy, or the Estonian area of the Baltic sea. Most of the presented results,
468 including the collection of the data, its processing using the reported methods,
469 the 3D reconstructions and the virtual scenarios developed with the aim of repli-
470 cating the experience of wreck exploration and survey, have been made possible
471 in the framework of the European FP7 project ARROWS.

472 **References**

- 473 [1] B. Allotta, S. Bargagliotti, L. Botarelli, A. Caiti, V. Calabrò, G. Casa,
474 M. Cocco, S. Colantonio, C. Colombo, S. Costa, M. Fanfani, L. Franchi,
475 P. Gambogi, L. Gualdesi, D. La Monica, M. Magrini, M. Martinelli, D. Mo-
476 roni, A. Munafò, G. Pace, C. Papa, M. Pascali, G. Pieri, M. Reggiannini,
477 M. Righi, O. Salvetti, M. Tampucci, Thesaurus project: Design of new
478 autonomous underwater vehicles for documentation and protection of un-
479 derwater archaeological sites, in: M. Ioannides, D. Fritsch, J. Leissner,
480 R. Davies, F. Remondino, R. Caffo (Eds.), Progress in Cultural Heritage
481 Preservation, Vol. 7616 of Lecture Notes in Computer Science, Springer
482 Berlin Heidelberg, 2012, pp. 486–493. doi:10.1007/978-3-642-34234-9_
483 50.
484 URL http://dx.doi.org/10.1007/978-3-642-34234-9_50
- 485 [2] B. Allotta, R. Costanzi, M. Magrini, N. Monni, D. Moroni, M. A. Pas-
486 cali, M. Reggiannini, A. Ridolfi, O. Salvetti, M. Tampucci, Towards a
487 robust system helping underwater archaeologists through the acquisition
488 of geo-referenced optical and acoustic data, in: L. Nalpantidis, V. Krger,
489 J.-O. Eklundh, A. Gasteratos (Eds.), Computer Vision Systems, Vol. 9163
490 of Lecture Notes in Computer Science, Springer International Publishing,

1
2
3
4
5
6
7
8
9
10
11
12
13
14
15
16
17
18
19
20
21
22
23
24
25
26
27
28
29
30
31
32
33
34
35
36
37
38
39
40
41
42
43
44
45
46
47
48
49
50
51
52
53
54
55
56
57
58
59
60
61
62
63
64
65

491 2015, pp. 253–262. doi:10.1007/978-3-319-20904-3_24.
492 URL http://dx.doi.org/10.1007/978-3-319-20904-3_24

493 [3] B. Allotta, R. Costanzi, A. Ridolfi, C. Colombo, F. B. M. Fanfani, F. Pazzaglia,
494 O. Salvetti, D. Moroni, M. A. Pascali, M. Reggiannini, M. Kruusmaa,
495 T. Salumäe, G. Frost, N. Tsiogkas, D. M. Lane, M. Cocco, L. Gualdesi,
496 D. Roig, H. T. Gündogdu, E. I. Tekdemir, M. I. C. Dede, S. Baines,
497 F. Agneto, P. Selvaggio, S. Tusa, S. Zangara, U. Dresen, P. Lätti, T. Saar,
498 W. Daviddi, The arrows project: adapting and developing robotics technologies for underwater archaeology, in: IFAC Workshop on Navigation, Guidance and Control of Underwater Vehicles, (NGCUV'2015), At Girona, Spain, 2015.
500
501 URL <http://hdl.handle.net/2158/1001621>

503 [4] X. Lurton, An introduction to underwater acoustics : principles and
504 applications, 1st Edition, Springer, 2002.
505 URL <http://www.amazon.com/exec/obidos/redirect?tag=citeulike07-20&path=ASIN/3540429670>

507 [5] D. T. Cobra, A. V. Oppenheim, J. F. Jaffe, Geometric distortions in
508 side-scan sonar images: A procedure for their estimation and correction, IEEE Journal of Oceanic Engineering 17 (1992) 252–268. doi:
509 10.1109/48.153442.
510

511 [6] M. Massot-Campos, G. Oliver-Codina, One-shot underwater 3d reconstruction, in: Emerging Technology and Factory Automation (ETFA), 2014
512 IEEE, 2014, pp. 1–4. doi:10.1109/ETFA.2014.7005282.
513

514 [7] R. C. Smith, K. S. Baker, Optical properties of the clearest natural waters
515 (200–800 nm), Appl. Opt. 20 (2) (1981) 177–184. doi:10.1364/AO.20.
516 000177.
517 URL <http://ao.osa.org/abstract.cfm?URI=ao-20-2-177>

518 [8] D. Lowe, Distinctive image features from scale-invariant keypoints, International Journal of Computer Vision 60 (2) (2004) 91–110. doi:10.1023/B:
519

1
2
3
4
5
6
7
8
9
10
11
12
13
14
15
16
17
18
19
20
21
22
23
24
25
26
27
28
29
30
31
32
33
34
35
36
37
38
39
40
41
42
43
44
45
46
47
48
49
50
51
52
53
54
55
56
57
58
59
60
61
62
63
64
65

520 VISI.0000029664.99615.94.
521 URL <http://dx.doi.org/10.1023/B%3AVISI.0000029664.99615.94>

522 [9] P. V. C. Hough, Machine Analysis of Bubble Chamber Pictures, in: In-
523 ternational Conference on High Energy Accelerators and Instrumentation,
524 CERN, 1959.

525 [10] D. H. Ballard, Readings in computer vision: Issues, problems, principles,
526 and paradigms, Morgan Kaufmann Publishers Inc., San Francisco, CA,
527 USA, 1987, Ch. Generalizing the Hough Transform to Detect Arbitrary
528 Shapes, pp. 714–725.
529 URL <http://dl.acm.org/citation.cfm?id=33517.33574>

530 [11] V. Pătrăucean, P. Gurdjos, R. von Gioi, A parameterless line segment
531 and elliptical arc detector with enhanced ellipse fitting, in: A. Fitzgibbon,
532 S. Lazebnik, P. Perona, Y. Sato, C. Schmid (Eds.), Computer Vision ECCV
533 2012, Lecture Notes in Computer Science, Springer Berlin Heidelberg, 2012,
534 pp. 572–585. doi:10.1007/978-3-642-33709-3_41.
535 URL http://dx.doi.org/10.1007/978-3-642-33709-3_41

536 [12] A. Desolneux, L. Moisan, J.-M. Morel, Gestalt theory and computer vision,
537 in: A. Carsetti (Ed.), Seeing, Thinking and Knowing, Vol. 38 of Theory
538 and Decision Library A:, Springer Netherlands, 2004, pp. 71–101. doi:
539 10.1007/1-4020-2081-3_4.
540 URL http://dx.doi.org/10.1007/1-4020-2081-3_4

541 [13] D. Moroni, M. Pascali, M. Reggiannini, O. Salvetti, Underwater scene un-
542 derstanding by optical and acoustic data integration, Proceedings of Meet-
543 ings on Acoustics (POMA) 17. doi:10.1121/1.4792225.

544 [14] D. Moroni, M. Pascali, M. Reggiannini, O. Salvetti, Underwater man-made
545 and archaeological object detection in optical and acoustic data, Pattern
546 Recognition and Image Analysis. Advance in Mathematical Theory and
547 Applications 24 (2014) 310–317. doi:10.1134/S1054661814020138.

1
2
3
4
5
6
7
8
9
10
11
12
13
14
15
16
17
18
19
20
21
22
23
24
25
26
27
28
29
30
31
32
33
34
35
36
37
38
39
40
41
42
43
44
45
46
47
48
49
50
51
52
53
54
55
56
57
58
59
60
61
62
63
64
65

548 [15] N. Mittal, D. Mital, K. L. Chan, Features for texture segmentation using
549 gabor filters, in: Seventh International Conference on Image Processing
550 And Its Applications 1999 (Conf. Publ. No. 465), Vol. 1, 1999, pp. 353–357
551 vol.1. doi:10.1049/cp:19990342.

552 [16] A. Jain, F. Farrokhnia, Unsupervised texture segmentation using gabor fil-
553 ters, in: IEEE International Conference on Systems, Man and Cybernetics,
554 1990, pp. 14–19. doi:10.1109/ICSMC.1990.142050.

555 [17] R. I. Hartley, A. Zisserman, Multiple View Geometry in Computer Vision,
556 2nd Edition, Cambridge University Press, ISBN: 0521540518, 2004.

557 [18] M. VARGA, Practical Image Processing And Computer Vision, Halsted
558 Press, New York, NY, USA, 2005.

559 [19] V. C. Lab, Meshlab: an open source 3d mesh processing system. (2008).
560 URL <http://meshlab.sourceforge.net/>

561 [20] D. Moroni, M. A. Pascali, M. Reggiannini, O. Salvetti, Curve recognition
562 for underwater wrecks and handmade artefacts, in: Proceedings of the 4th
563 International Workshop on Image Mining. Theory and Applications, 2013,
564 pp. 14–21. doi:10.5220/0004392300140021.